scientific reports

Check for updates

OPEN

Structural, elastic, electronic, magnetic and thermal properties of X_3FeO_4 (X = mg, ca and Sr) materials

Mohammed El Amine Monir[1], Abdelkarim Bendoukha Reguig[1], M. A. Ghebouli[2,3], K. Bouferrache[4], Faisal Katib Alanazi[5]✉, M. Fatmi[2]✉ & H. Bouandas[6]

This prediction evaluates the different physical characteristics of magnetic materials X_3FeO_4 (X = Mg, Ca and Sr) by using density functional theory (DFT). The generalized gradient approximation (GGA) approach is chosen to define the exchange and correlation potential. The structural study of the compounds X_3FeO_4 (X = Mg, Ca and Sr) shows that the ferromagnetic phase is the more stable ground state, where all the parameters of the network are given at equilibrium. The calculated elastic constants confirm their stability in the cubic structure. The electronic characteristics calculated using the GGA and GGA + U approaches prove that all these compounds are semi-metallic with a wide band gap (E_{HM}) and a high Curie temperature (T_C). Furthermore, the magnetic moments of the studied compounds are calculated in order to claim their half-metallicity behavior. The *p-d* hybridization between the *3d*-Fe and *2p*-O states generates weak magnetic moments in the non-magnetic X and O sites, and decreases the Fe atomic moment relative to its free space charge of 4 μ_B. The thermal parameters including the thermal expansion coefficient, the heat capacity at constant volume and the Debye temperature were calculated for these compounds.

Keywords X_3FeO_4 (X = mg, ca and Sr) compounds, Elastic constants, Half-metallic gap, Curie temperature, Magnetic moments, GGA + *U*, FP-L/APW + lo

The discovery of new magnetic materials is increasingly helping the technology, including spintronics and optoelectronics. During this decade, the aim goal of scientists in the spintronic field is to find new magnetic materials with a high Curie temperature in order to manufacture devices capable of storing information. According to the researchers, the excellent magnetic material for making a durable spintronic device is the half-metal. The half-metallic material has a metallic behavior in one spin direction and a semiconductor behavior in the other spin direction, lead to 100% spin-polarization at the Fermi level[1]. The half-metallicity domain was virgin before the prediction of Groot et *al.*, which calculates for the first time the electronic structure of PtMnSb and NiMnS half-Heusler alloys[2]. After Groot's prediction, many interesting theoretical and experimental works in the spintronic field were carried out such as perovskite alloys Sr_2FeMoO_6[3], $La_{0.7}Sr_{0.3}MnO_3$[4] and Heusler alloys Co_2FeSi[5] and Co_2MnSi[6]. We note that the work of Ohno et al. in 1996, which is based on the discovery of ferromagnetism in semi-Heusler at a Curie temperature above 100 K[7], presents significant results on pnictide and chalcogenide semiconductors doped with transition metals (TM). Recently, researchers have shown that semi-metallic materials belong to new magnetic materials from different families, such as perovskites PrMnO3 and ortho-manganite NdMnO3, where DFT analyzes their mechanical, thermal and thermoelectric properties[8]. A computational study of the optoelectronic and thermoelectric properties of new perovskite materials XAlN3 (X = K, Rb, Cs) shows semi-metallic behavior[9]. The presence of ferromagnetism is reported in the semi-metallic double perovskites Pb2XX'O6 (X = V and Cr and X'=Zr and Hf)[10] and in the semi-metallic Heusler alloys CrYCoAl[11]. A study of the structural parameters, electronic structure, magnetic and mechanical properties of

[1]Faculty of the Exact Sciences, Mustapha Stambouli University of Mascara, B.P. 305, 29000 Mascara, Algeria. [2]Research Unit on Emerging Materials (RUEM), University Ferhat Abbas of Setif 1, Setif 19000, Algeria. [3]Department of Chemistry, Faculty of Sciences, University of Mohamed Boudiaf, M'sila 28000, Algeria. [4]Department of Physics, Faculty of Sciences, University of Mohamed Boudiaf, M'sila 28000, Algeria. [5]Department of Physics, college of Sciences, Northern Border University, P.O. Box 1321, Arar 91431, Saudi Arabia. [6]Applied Optics Laboratory, Institute of Optics and Precision Mechanics, University Setif 1, Setif 19000, Algeria. ✉email: Faisal.katib.al@gmail.com; fatmimessaoud@yahoo.fr

solid semi-metallic compounds Heusler Cr2VA[12]. A theoretical and experimental study was carried out on the magnetic and electronic properties of the Heusler Mn-Co-V-Al semi-metallic alloy[13]. We note the work on semiconductors doped with TM such as bipolar magnetic semiconductors and semimetals in transition metals doped with zigzag nanoribbons SnSe2[14]. The induction of semi-metallic ferromagnetism in BaS semiconductor by Cr doping[15] and high Curie temperature and semi-metallic ferromagnetism in Cr and V doped ZnSe in wurtzite phase. A study of nitrogen-induced semimetallic ferromagnetism in alkali metal oxides[16] and in calcium and cadmium oxides[17]. Ferromagnetism in AlP doped with alkali metals by ab initio[18] and in metal oxides such as magnesium[19]. A study of the magneto-electronic and elastic properties of the photovoltaic halide semiconductor (RbGeI3) and ferromagnetic metal oxide semiconductor (RbDyO3)[20] was carried out. Recently, the half-metallic ferromagnetism is reported in new materials that have a perovskite structure such as $ZnCrO_3$[21], the double halide perovskites Cs_2AgMBr_6 (M = V, Mn, Ni)[22] and the lead free half-metallic double perovskites $Li_2Mo(Cl/Br)_6$[23]. High performance for half metallicity of quadruple perovskite oxide $DyCu_3Fe_2Re_2O_{12}$ synthesis at high pressure[24] and tunability of half metallicity and thermoelectric indicators in Na_2TaX_6 (X = Cl, Br) vacancy ordered double perovskites[25]. The alkali-metal oxides A_3BO_4 (A = alkali metal, B = metal or nonmetal) crystallizes in the cubic system under the space group $Pm\bar{3}m$ are classified as metals and semiconductors[26].

In this research, we studied the structural, elastic, electronic, magnetic and thermal properties of cubic alkali-metal oxides Mg_3FeO_4, Ca_3FeO_4 and Sr_3FeO_4 with the aim of proving their mechanical and structural stabilities and also to show that they are new half-metallic materials with a large half-metallic gap and a high Curie temperature. This study shows that alkali-metal oxide materials (X_3FeO_4 (X = Mg, Ca and Sr)) can exhibit half-metallic behavior depending on their clear half-metallic gap as well as their Curie temperature.

The aim objective of this work is to show the half-metallic nature within these magnetic materials X_3FeO_4 (X = Mg, Ca and Sr) through the treatment of their structural, electronic and magnetic properties by using the full-potential linearized augmented plane waves with local orbitals (FP-LAPW + lo) method.

The important motivation in this work is to found a large half-metallic gap and a high Curie temperature of Mg_3FeO_4, Ca_3FeO_4 and Sr_3FeO_4 alkali-metal oxides, by employing GGA and GGA + *U* parameterizations, where the GGA + *U* calculation is added in order to improve more half-metallic gap and Curie temperature.

The remainder of this paper is ordered as follows: Sect. "Computational detail" presents the computational details reported in this study. Section "Discussion on results" reveals the main results obtained and their discussions when calculating the structural, elastic, electronic and magnetic properties. Finally, the summary of the main findings is given in Sect. "Conclusions".

Computational detail

We integrate the precise technique of linearized augmented plane wave full potential plus local orbitals (FP-LAPW + lo)[27,28] in the WIEN2k code[29] and based on the density functional theory (DFT)[30], to predict various physical properties of X_3FeO_4 (X = Mg, Ca, and Sr). The exchange and correlation potential were determined using the generalized gradient approximation of Perdew–Burke–Ernzerhof[31].

The various computational parameters included in this method are listed as follows: the matrix size parameter that converges the energy eigenvalues and extends the plane waves is called $R_{MT}\times K_{max}$. R_{MT} stands for the minimum radius of muffin-tin spheres, and K_{max} for the maximum modulus of the reciprocal lattice vector; it was equal to 8. The translation of the charge density and the expansion of the wave functions are determined by Fourier expansion term (G_{Max}), it was chosen G_{Max} = 12 $(Ry)^{1/2}$. The enormous magnitude of the angular momentum of the muffin-tin spheres is equal to l_{max} = 10. The cut-off energy ($E_{cut-off}$) gives the number of plane wave functions being utilized as basic functions to represent the wave function is taken $E_{cut-off}$ = -6 eV. The Brillouin zone (BZ) integration creates 56 k-points in the irreducible Brillouin zone, where it is based on the 12 × 12 × 12 mesh. The sphere radii of different atoms of Mg, Ca, Sr, Fe, O1 and O_2 are taken as 1.90, 2.09, 2.25, 1.76 and 1.76 a.u., respectively. The structural parameters of all compounds are relaxed before starting the calculations. The electronic and magnetic properties were computed using the GGA + U approximation (U is the Hubbard parameter which estimates the Coulomb repulsion coming from the delocalized orbitals d and f)[32]. The effective Hubbard term of the Fe atom (U_{eff} = *U-J*) was optimized with respect to the integer value of the total magnetic moment corresponding to each studied half-metallic material, it was found U_{eff} = 5.3 eV for the three studied materials. We neglect the Hubbard parameter for the Mg, Ca and Sr elements because they are not magnetic atoms. The process of anti-ferromagnetic (AFM) calculations is carried out following the orientations of the magnetic moments of the Fe atom within the unit cell of 1 × 1 × 1 dimension, where the atoms (0, 0, 0), (0, 1, 0), (1, 0, 0) and (1, 1, 0) are oriented downward, while the atoms (0, 0, 1), (0, 1, 1), (1, 0, 1) and (1 ,1, 1) are oriented upwards. Therefore, this orientation of the magnetic moment corresponds to the configuration of AFM-type I. Based on the density-functional perturbation theory, the phonon dispersion curves of the studied compounds have been determined by applying the dynamic lattice calculations within the PHONOPY package[33].

Discussion on results

Structural properties

Crystal system

The alkali metal oxides A_3BO_4 type have a cubic crystal structure identified by the space group $Pm\bar{3}m$ (no. 221)[27]. The Wyckoff positions 3c (0, ½, ½), 1a (0, 0, 0), 3d (0, 0, ½) and 1b (½, ½, ½) in this crystal structure are occupied by A, B, O1 and O2 atoms, respectively[26].

Lattice parameters at the equilibrium

The treatment of structural properties was done by adopting the Birch-Murnaghan equation of state (EOS)[34,35]; where the process is carried out by minimizing the total energy of the compound as a function of its cellular volume at each magnetic phase. In this prediction, we have optimized the total energy of all Mg_3FeO_4, Ca_3FeO_4 and Sr_3FeO_4 compounds taken in their non-magnetic (NM), ferromagnetic (FM) and anti-ferromagnetic (AFM) phases. The *E-V* curves for each compound are reported in Fig. 1. So, the GGA calculations show that

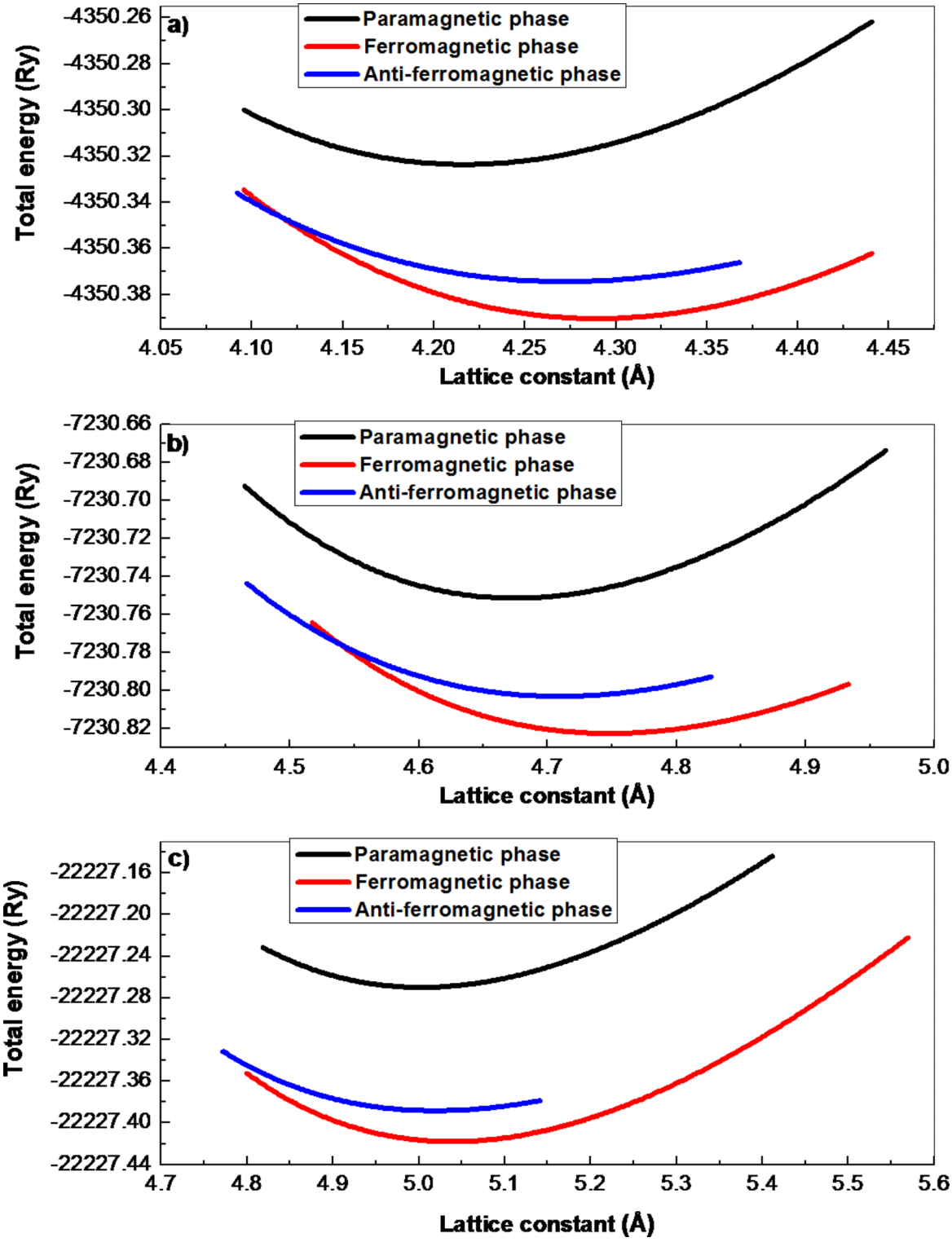

Fig. 1. Optimization of the total energy as a function of the lattice constant for (**a**) Mg_3FeO_4, (**b**) Ca_3FeO_4 and (**c**) Sr_3FeO_4 compounds.

Compound	Phase	Lattice constant a_0 (Å)	Bulk modulus B_0 (GPa)	B'	Minimum of total energy E_0 (Ry)
Mg_3FeO_4	PM phase	4.2166	169.3120	4.3556	-4350.323693
	FM phase	4.2898	152.0035	3.1548	-4350.390455
	AFM phase	4.2712	155.3142	3.7985	-4350.374465
Ca_3FeO_4	PM phase	4.6748	119.4981	4.4163	-7230.751362
	FM phase	4.7480	108.9531	3.2138	-7230.822512
	AFM phase	4.7091	115.3257	3.6954	-7230.803145
Sr_3FeO_4	PM phase	5.0017	97.1127	4.9957	-22227.270220
	FM phase	5.0385	94.3614	4.4637	-22227.418098
	AFM phase	5.0195	96.3892	4.7125	-22227.388579

Table 1. Optimized lattice parameters of X_3FeO_4 (X = mg, ca and Sr) compounds at equilibrium, using the GGA approximation.

Compound	E_0	E_X	E_{Fe}	E_O	E_f	E_{Coh}
Mg_3FeO_4	-4350.390455	-400.559922	-2545.132819	-150.116889	-3.110314	2.748663
Ca_3FeO_4	-7230.822512	-1360.659386	-2545.132819	-150.116889	-3.243979	3.031704
Sr_3FeO_4	-22227.418098	-6359.595214	-2545.132819	-150.116889	-3.032081	2.700109

Table 2. The GGA calculations of the formation energy E_f (in Ry) and the cohesive energy (in Ry) for the X_3FeO_4 (X = mg, ca and Sr) compounds, taken in their stable ferromagnetic ground state.

the ferromagnetic (FM) configuration is the most stable state of all the studied materials. On the other hand, the equilibrium lattice parameters of these compounds, such as lattice constant (a_0), bulk modulus (B_0) and its first pressure derivative (B') taken at all magnetic phases are computed using the GGA approximation and reported in Table 1. We can claim that these structural results are original and of much greater utility for future experimental projects in the field of spintronics.

Formation energy and cohesive energy

The formation energy (E_f) of a material is defined as the energy required to hold the material stable in its crystalline structure at the theoretical temperature (0 K). The negative sign of E_f proves that the material is stable in its own structure and confirms more and more that the bonds which bind the atoms to their favorable crystal are increasingly strong[36]. Moreover, E_f energies of all X_3FeO_4 (X = Mg, Ca and Sr) alkali metal oxides are calculated using the following formula[37,38].

$$E_f\left(X_3FeO_4\right) = E_0 - \left(3E_X + E_{Fe} + 4E_O\right) \tag{1}$$

Where E_0 represents the total energy of the material and E_X, E_{Fe} and E_O denote the energies of the individual X, Fe and O atoms taken in their stable crystal system, respectively. Based on the GGA calculations, the computed E_f term of all X_3FeO_4 (X = Mg, Ca and Sr) compounds are listed in Table 2; therefore, all the studied compounds were confirmed to be stable in their crystal structure due to the negative sign of their E_f term (see Table 2).

The cohesive energy (E_{Coh}) is defined as a measure of the strength of forces that bind atoms together in the solid. For the cubic A_3BO_4 compounds, E_{Coh} is the difference in the total energy of the constituent atoms at infinite separation and the total energy of the compound at particular phase:

$$E_{Coh}\left(X_3FeO_4\right) = \left(3E^X + E^{Fe} + 4E^O\right) - E_0 \tag{2}$$

Here, E^X, E^{Fe} and E^O are the atomic energies of X, Fe and O atoms, respectively; whereas, E_0 denotes the total energy of the system. The computed E_{Coh} values of the studied materials are reported in Table 2.

Dynamic stability

The phonon dispersion curves of all X_3FeO_4 (X = Mg, Ca and Sr) compounds are displayed in Fig. 2 along the *R-Γ-X-Z-M-Γ* path in the three-dimensional (3D) Brillouin zone. The absence of imaginary frequency modes (frequencies with a negative sign) in the phonon dispersion curves of all the compounds proves their dynamic stability.

Elastic properties

The elasticity in materials is the response to stresses exerted on the material; the relationship between stress (σ) and strain (ε) is given by Hook's law[39]:

$$\begin{pmatrix} \sigma_{11} \\ \vdots \\ \sigma_{11} \end{pmatrix} = \begin{pmatrix} C_{11} & \cdots & C_{16} \\ \vdots & \ddots & \vdots \\ C_{61} & \cdots & C_{66} \end{pmatrix} \begin{pmatrix} \epsilon_{11} \\ \vdots \\ \epsilon_{11} \end{pmatrix} \tag{3}$$

Where, C_{ij} are the elastic constants expressed in GPa.

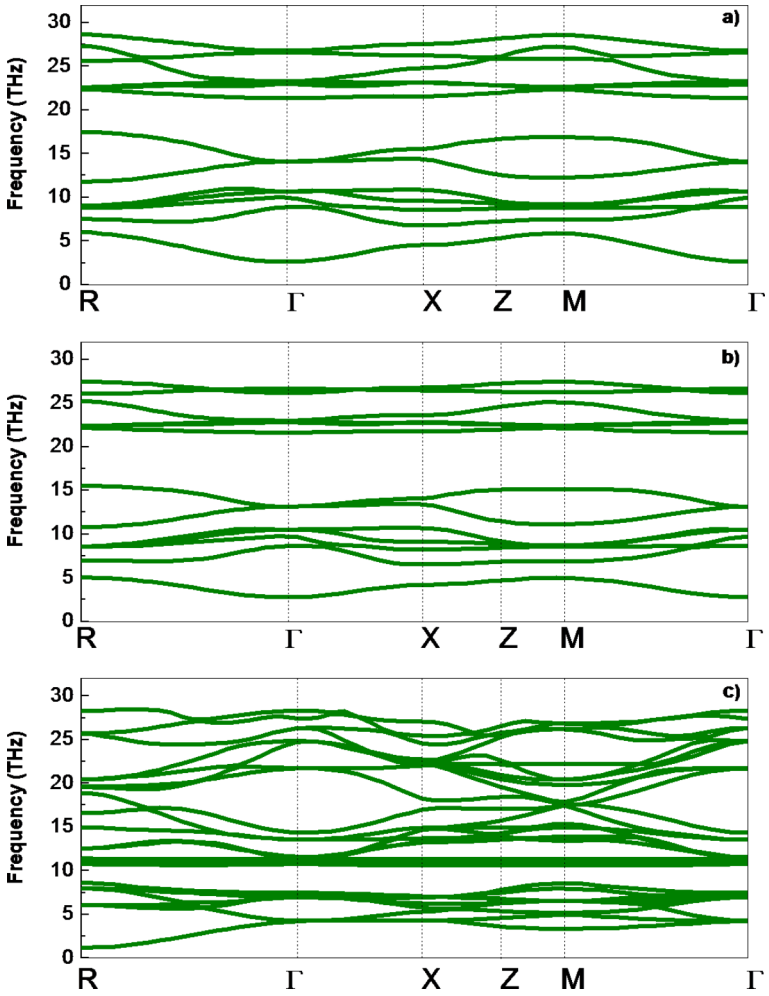

Fig. 2. The phonon dispersion of (**a**) Mg_3FeO_4, (**b**) Ca_3FeO_4 and (**c**) Sr_3FeO_4 compounds, along *R-Γ-X-Z-M-Γ* path.

Compound	C_{11}	C_{12}	C_{44}	B_0	A	ξ	G	B_0/G	υ
Mg_3FeO_4	254.6122	102.5119	117.3542	153.2120	1.5431	0.5408	98.6211	1.5535	0.2350
Ca_3FeO_4	244.8110	57.6098	101.2135	120.0102	1.0813	0.3858	98.0964	1.2234	0.1788
Sr_3FeO_4	181.6935	51.8139	88.6267	95.1071	1.3647	0.4334	78.2472	1.2155	0.1772

Table 3. Calculations of the elastic constants C_{ij} (in GPa), the bulk modulus B_0 (in GPa), the elastic anisotropy *A*, the Kleinman parameter ξ, the shear modulus *G*, the Pugh's ratio B_0/G and the Poisson's ratio (*υ*) for the X_3FeO_4 (X = mg, ca and Sr) compounds taken in their stable ferromagnetic ground state, using the GGA approximation.

In cubic system, the elasticity tensor is composed of three types of elastic constants such as C_{11}, C_{12} and C_{44}. In this work, we have determined the elastic constants (C_{11}, C_{12} and C_{44}) for the equilibrium Mg_3FeO_4, Ca_3FeO_4 and Sr_3FeO_4 compounds by using IRelast program[40] implemented in the WIEN2*k* code[29], where the results of elastic constants are developed by the GGA approximation and grouped in Table 3. A material is mechanically stable if its elastic constants must obey to Born's criteria[41,42]. In fact, the Born criteria for the cubic system are given as follows[41,42]:

$$\begin{cases} (C_{11} - C_{12}) > 0 \\ (C_{11} + 2C_{12}) > 0 \\ C_{11} > 0 \\ C_{44} > 0 \\ C_{12} < B < C_{11} \end{cases} \quad (4)$$

After checking, the GGA calculations show that all the X_3FeO_4 (X = Mg, Ca and Sr) compounds are mechanically stable.

The Zener elastic anisotropy (A) is defined for the cubic system as follows[43]:

$$A = \frac{2C_{44}}{C_{11} - C_{12}} \tag{5}$$

A material is elastically isotropic if its anisotropy factor equals to unity ($A = 1$); outside this value, the material becomes anisotropic[43]. The values of the anisotropy factor for the equilibrium X_3FeO_4 (X = Mg, Ca and Sr) compounds are calculated through the GGA approximation and reported in Table 3. We can conclude that these materials are elastically anisotropic.

The shear modulus (G) is an important factor which evaluates the resistance to plastic strain; it is defined as the average of the Voigt[44], and Reuss[45] approaches, it is expressed according to the Hill's approach[46]:

$$G = \frac{G_V + G_R}{2} \tag{6}$$

Where,

$$\begin{cases} G_V = \frac{C_{11} - C_{12} + 3C_{44}}{5} \\ G_R = \frac{5C_{44}(C_{11} - C_{12})}{4C_{44} + 3(C_{11} - C_{12})} \end{cases} \tag{7}$$

The bulk modulus (B_0) is another parameter that estimates the resistance to the fracture[47]. The Pugh's ratio (B_0/G) is a factor that describes the brittleness and ductility of materials[48,49]. The material is considered as brittle when B_0/G factor is less than 1.75; on the other side, the material becomes as ductile. According to the Pugh's ratio values reported in Table 3, the studied compounds are confirmed to be brittle materials.

The Poisson's ratio (υ) is an elastic parameter which describes the type of bonding force between the constituents of the solid. It can be calculated for each cubic material according to the following formula[50]:

$$\upsilon = \frac{3B - 2G}{2(3B + G)} \tag{8}$$

The ratio υ varies between 0.25 and 0.5. When the ratio υ is greater than 1/3, a ductile material is obtained, and when it is less than 1/3, the material becomes brittle[50]. The computed values of the ratio υ are reported in Table 3. So, all the studied compounds are found as brittle materials.

During volume-conserving distortions, the arrangement of cation and anion sublattices is described by the Kleinman parameter (ξ)[51]. Thus, it shows the ability of the material to resist against stretching and bending, suggesting stability[51]. Kleinman parameter (ξ) is expressed in the following relation[51]:

$$\xi = \frac{C_{11} + 8C_{12}}{7C_{11} + 2C_{12}} \tag{9}$$

In fact, the ξ parameter varies from 0 to 1. For a material under stress, its Kleinman parameter is equal to zero ($\xi = 0$), this means that the bond stretching is more critical than the bond bending. Table 3 reports the computed ξ parameter for the X_3FeO_4 (X = Mg, Ca, and Sr) compounds. It is evident that the ξ values of the Sr_3FeO_4 and Ca_3FeO_4 compounds calculated with the GGA scheme are less than 0.5, which can be attributed to the presence of bond stretching and bond bending which give to the compounds their mechanical strength, where the stretching of the bonds appearing to be slightly dominant. For the compound Mg_3FeO_4, the ξ parameter is found above 0.5, confirming that bond bending is slightly dominant.

Electronic properties

The electronic structures of the equilibrium X_3FeO_4 (X = Mg, Ca and Sr) compounds were performed using the PBE-GGA and GGA + U approximations in order to know the mechanism of half-metallicity within these materials and to predict their electronic and magnetic usefulness in future research.

Equilibrium electronic structure

The spin-polarized electron band structures and total density of states (TDOS) of the equilibrium Mg_3FeO_4, Ca_3FeO_4 and Sr_3FeO_4 compounds were calculated by PBE-GGA and GGA + U settings and illustrated in Figs. 3, 4 and 5, respectively. In fact, the electronic band structures are depicted along the high symmetry directions of the first Brillouin zone. Firstly, we observe a large exchange-splitting between spin-up (minority spin) and spin-down (majority spin) electrons; where this proves the magnetic nature of these compounds. In all the studied compounds, both GGA and GGA + U calculations show that the spin-up band structures have a semiconductor character, while their spin-down band structures are identified by the metallic behavior, where these results confirm the half-metallic nature that characterizes these compounds. We can conclude that these materials are complete half-metals and 100% spin-polarized at the Fermi level (E_F).

The energy of half-metallic gap (E_{HM}) is defined as the minimum between the lowest energy of the majority-spin and minority-spin conduction bands with respect to the Fermi level, and the absolute values of the highest energy majority-spin and minority-spin valence bands[52,53]. The calculated half-metallic gap energy (E_{HM}) and the spin-up gap energy (E_g) of these compounds are listed in Table 4. It is obvious to note that the E_{HM}

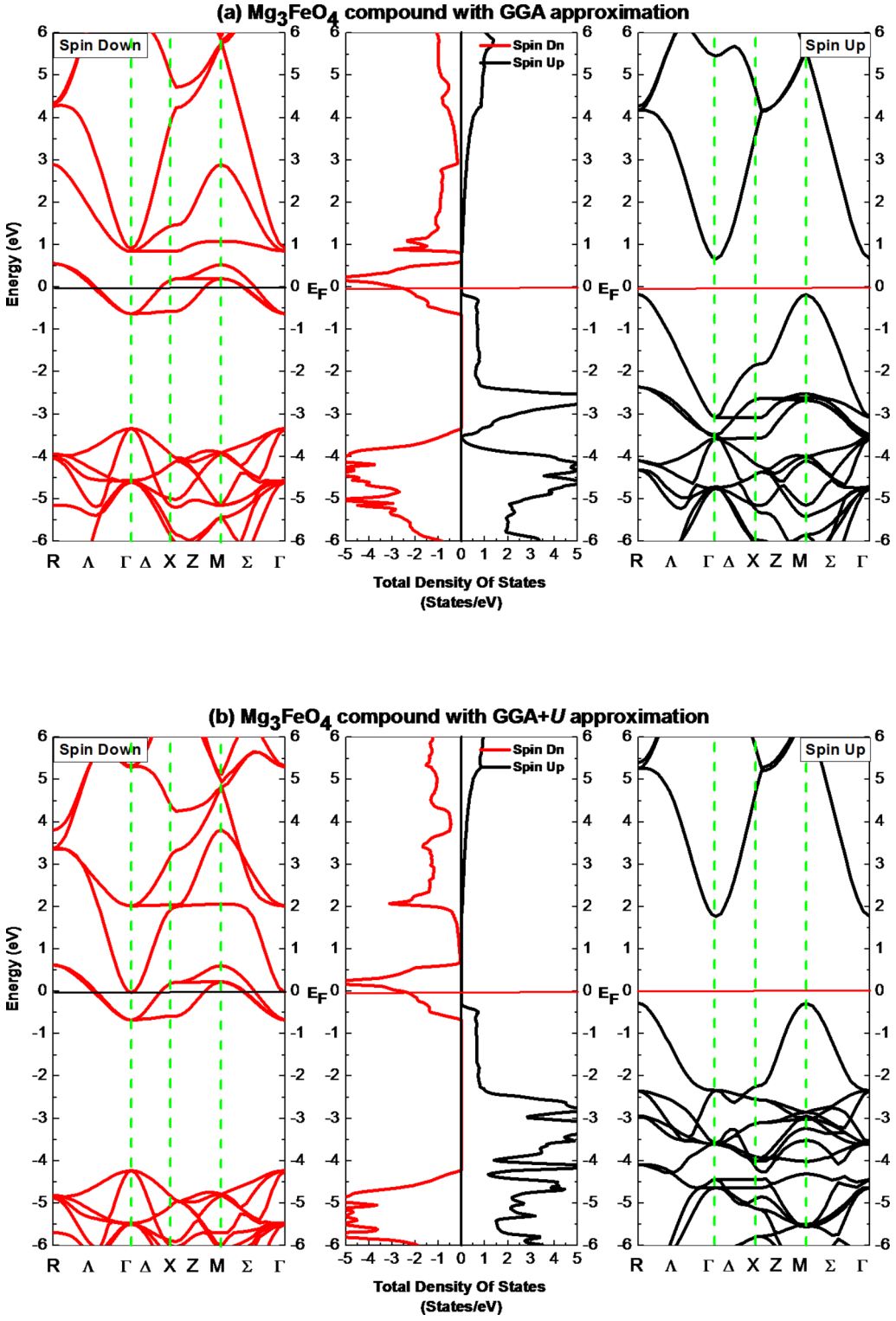

Fig. 3. Development of the spin-polarized total density of states (TDOS) and band structure of the material Mg_3FeO_4, applying the (**a**) PBE-GGA and (**b**) GGA + *U* parameterizations.

values achieved by the GGA + *U* calculations are the most approved due to the presence of a wider half-metallic gap compared to those of the GGA calculations; therefore, the studied compounds can be used in spintronic application due to half metallic property and with wide band gap it can operate at higher temperature. Moreover, a widened gap promises high Curie temperature for manufacturing spintronic devices.

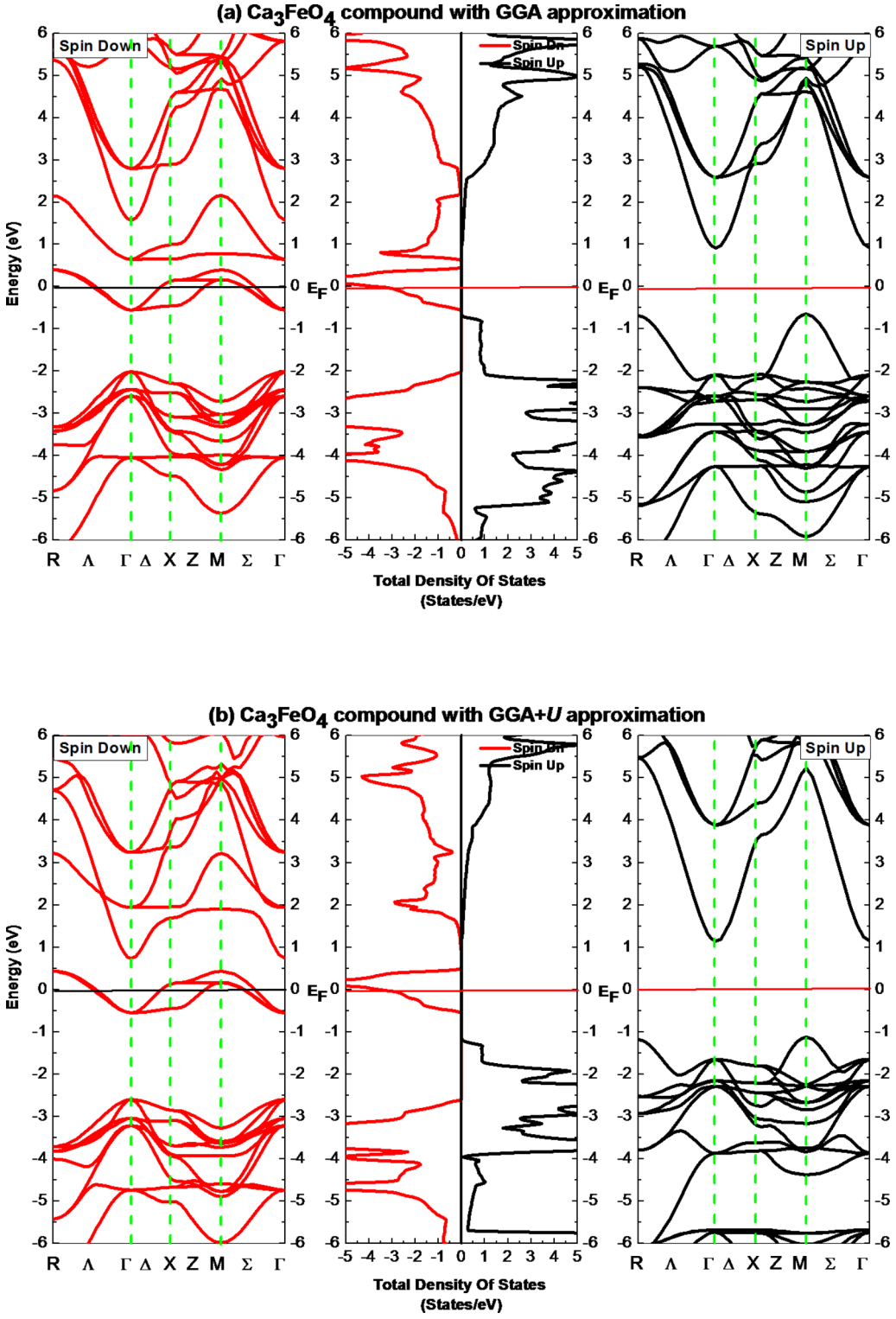

Fig. 4. Development of the spin-polarized total density of states (TDOS) and band structure of the material Ca_3FeO_4, applying the (**a**) PBE-GGA and (**b**) GGA + *U* parameterizations.

Density of states projections

The partial densities of states (PDOS) calculations are obvious to know the orbital contributions of the electronic structure formation. The PDOS curves of the different equilibrium compounds Mg_3FeO_4, Ca_3FeO_4 and Sr_3FeO_4 are developed by the GGA and GGA + *U* approximations and depicted in Figs. 6, 7 and 8, respectively.

For the equilibrium Mg_3FeO_4 compound, calculations of the GGA + *U* approximation show that the DOS is mainly contributed by the *3d*-Fe states with smaller contributions coming from the *2p*-O1 and *2p*-O2 orbitals.

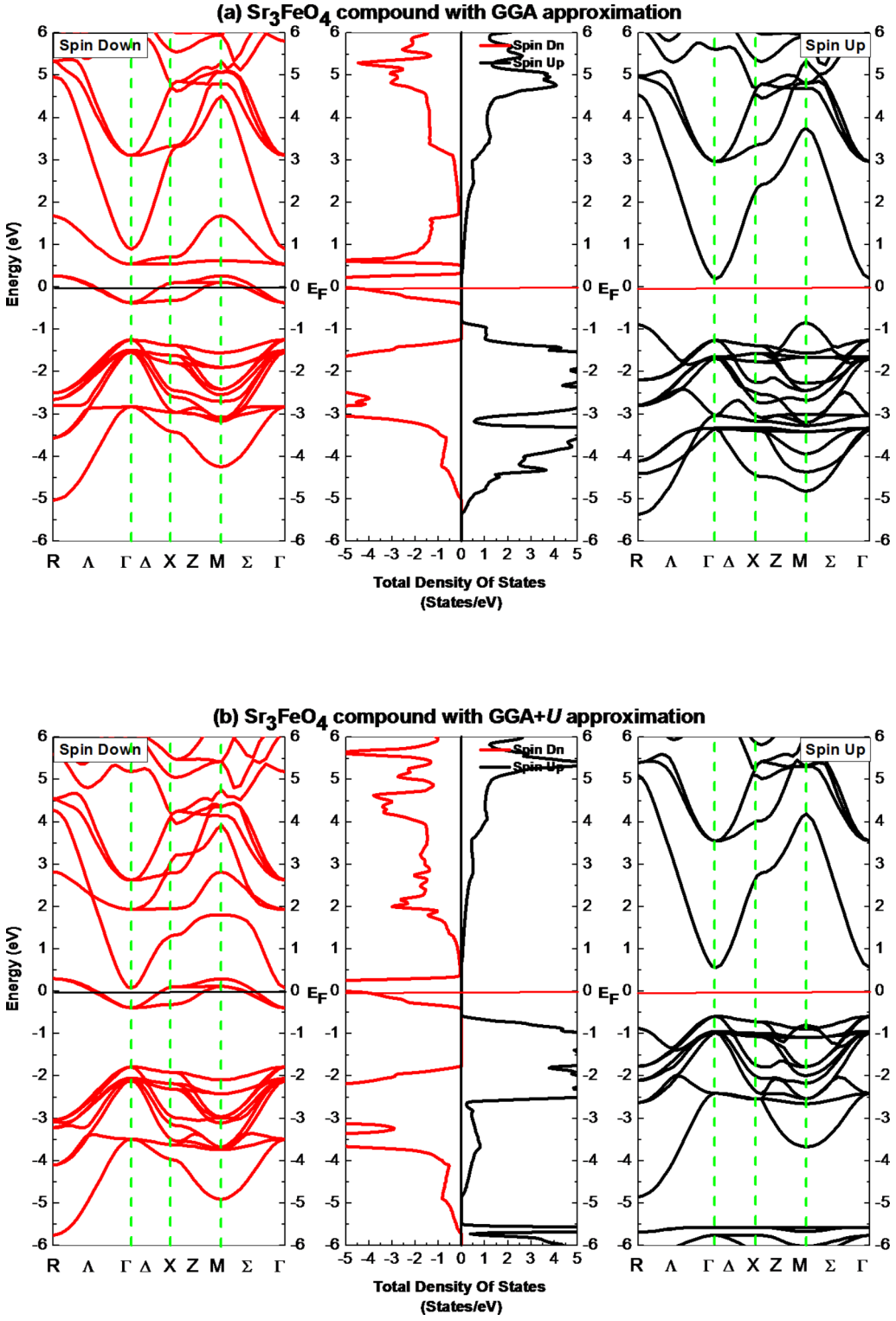

Fig. 5. Development of the spin-polarized total density of states (TDOS) and band structure of the material Sr_3FeO_4, applying the (**a**) PBE-GGA and (**b**) GGA + *U* parameterizations.

The spin-up and spin-down energy bands between −8 and −3.5 eV belong to the *3d*-Fe, *2p*-O1 and *2p*-O2 electrons, while the energy bands in the ranges between −3.5 and E_F for spin-up direction and between −0.5 and 3 eV for spin-down direction arising only from *3d*-Fe states. According to these results, we can demonstrate that the *3d*-Fe electrons are responsible for the half-metallic process within this material because they occupy the spin-down bands in the energy range around the Fermi level and create an energy gap in the same range for

Compound	E_{HM}	E_g
Mg_3FeO_4	0.1220 (0.2894)	0.8708 (2.0681)
Ca_3FeO_4	0.6385 (1.1411)	1.5511 (2.2858)
Sr_3FeO_4	0.2547 (0.5633)	1.0340 (1.1973)

Table 4. Calculations of the half-metallic gap energy E_{HM} (in eV) and the spin-up band gap energy E_g (in eV) for the X_3FeO_4 (X = mg, ca and Sr) compounds, the values of GGA + *U* are between brackets.

the spin-up direction. Moreover, a strong hybridization is observed between the *2p*-O1, *2p*-O2 and *3d*-Fe states in the energy range from − 8 to -3.5 eV for spin-up and spin-down directions.

The GGA + *U* calculations of the equilibrium Ca_3FeO_4 compound prove that: the *3d*-Fe states are the origin of the energy bands located in the regions between − 6.5 and − 0.5 eV for spin-up component and between − 0.5 and 2.2 eV for spin-down component; the *2p*-O1 and *2p*-O2 bands are located in the spin-up and spin-down energy spectrum between − 6.5 and − 2 eV. We notice robust hybridization between the *2p*-O1, *2p*-O2 and *3d*-Fe states in the energy range between − 6.5 and − 2 eV.

Based on the GGA + *U* calculations performed within the equilibrium Sr_3FeO_4 compound, the energy bands belong to the spin-up range from − 5 to -1 eV and the spin-down range from − 0.4 to 2 eV come from the *3d*-Fe electrons; the energy spectrum bands between − 5 and − 1.1 eV come from the *2p*-O1 and *2p*-O2 orbitals. Furthermore, a strong hybridization between the *2p*-O1, *2p*-O2 and *3d*-Fe states is located in the energy range from − 5 to -1.1 eV.

Depending on the crystal field effects[54], the *3d*-Fe states are divided into doubly degenerate e_g states and triply degenerate t_{2g} states, where the e_g energy levels are lower than the t_{2g} energy levels[55]. The Fe element has six electrons in its *d* orbital, five of them occupy the majority-spin of e_g and t_{2g} states, while the remaining electron fills the minority-spin of e_g states, where the result of this exchange and splitting process is a number of four single electrons which corresponds exactly to the total magnetic moment found for each material.

In the end, we can conclude that the *3d*-Fe states of all the studied compounds are responsible for their half-metallicity because they occupy the spin-down bands in the energy range around the Fermi level, and they are therefore responsible for producing an energy gap in the same range following the spin-up direction.

Magnetic properties

Magnetic moments

The GGA and GGA + *U* approximations were applied in this research to calculate different magnetic moments of the studied compounds, such as: the total magnetic moment of the compound (M_T), the interstitial magnetic moment of the interstitial area and the local magnetic moment of each site of X, Fe, O1 and O2 atoms, where the computed values are listed in Table 5. The total magnetic moment of all the studied compounds computed by the GGA and GGA + *U* schemes is found with an integer value of 4 μ_B, where this result confirms the full half-metallic nature that reigns within these materials. According to the GGA and GGA + *U* approximations, the main contribution to the total magnetic moment of all the studied X_3FeO_4 (X = Mg, Ca and Sr) compounds comes from the Fe atom with slight contributions coming from O1 atom. The atomic magnetic moments of X and Z atoms are given in opposite signs, this is due to the anti-parallel interaction between the valence electrons of X and Fe atoms during the exchange and splitting process. Furthermore, due to the *p-d* hybridization between the *3d*-Fe and *2p*-O orbitals, weak magnetic moments are introduced in the non-magnetic X, O1 and O2 sites and the Fe atomic magnetic moment was reduced compared to its free space charge of 4 μ_B.

Curie temperature

The Curie temperature (T_C) for magnetic materials is the critical temperature that separates the ferromagnetic and the non-magnetic regimes. The T_C can be estimated for the equilibrium X_3FeO_4 (X = Mg, Ca and Sr) compounds using the method below[56]:

$$K_B T_C = \frac{2}{3} \sum_{i \neq j} J_{ij} \tag{10}$$

Where J_{ij} parameter denotes the exchange interactions, it can be determined by the following relation:

$$J_{ij} = \frac{|E_{FM} - E_{AFM}|}{2} \tag{11}$$

Table 5 presents the T_C values for the studied compounds, developed by the GGA approximation. We found that the estimated T_C corresponding to each studied compound is higher.

Thermal properties and sound velocities

Thermal properties

The thermal properties of the studied materials were also calculated in order to know the evolution of the different thermal parameters appropriate to these materials as a function of temperature. The thermal expansion coefficient (α), the heat capacity at constant volume (C_V) and the Debye temperature (θ_D) of the different studied materials were computed by using the GIBBS program founded on the quasi-harmonic Debye model[57]. Based on

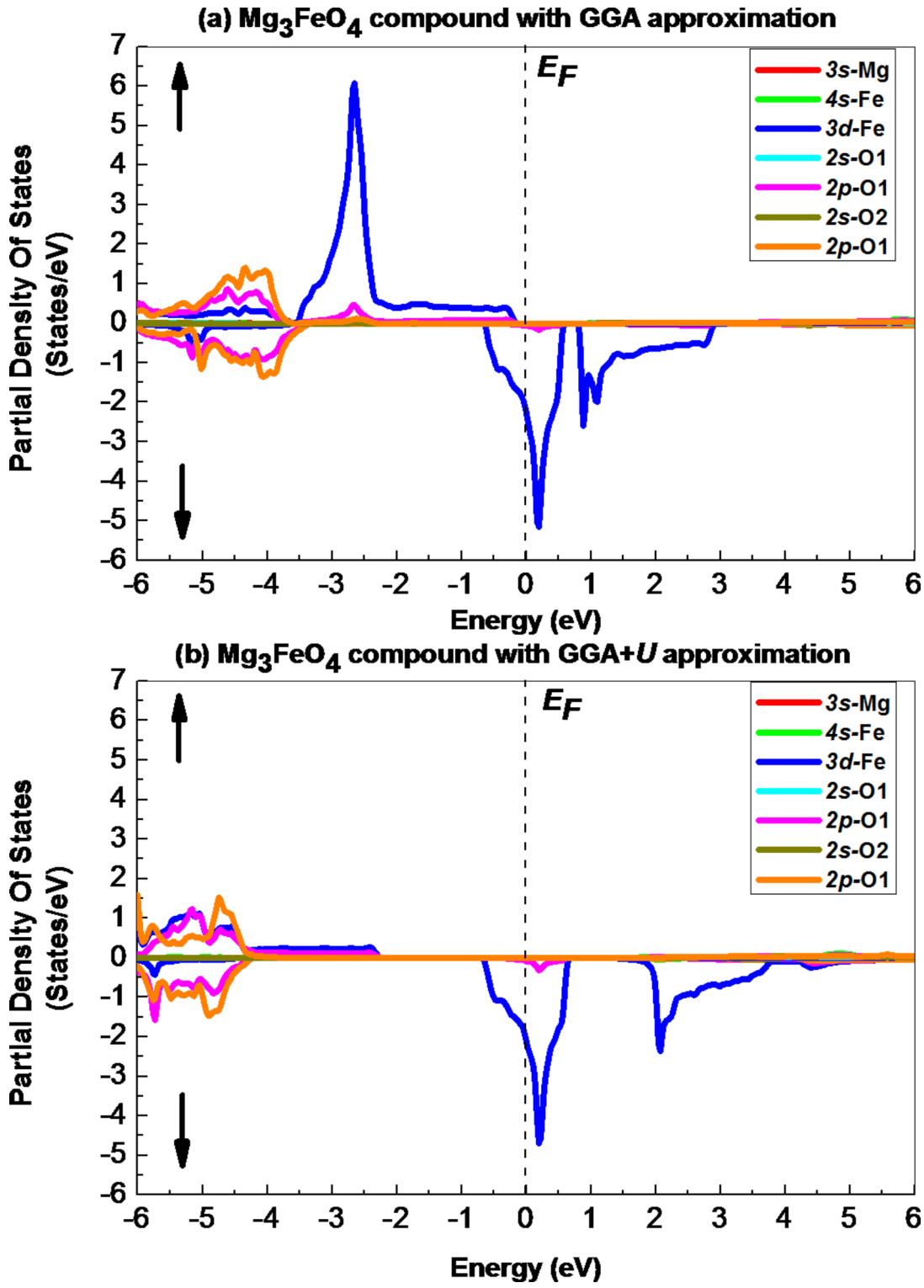

Fig. 6. Calculation of the spin-dependent partial density of states (PDOS) of the material Mg_3FeO_4, applying the (**a**) PBE-GGA and (**b**) GGA + *U* schemes.

the GGA calculations, the variation of α, C_V and θ_D of the equilibrium X_3FeO_4 (X = Mg, Ca and Sr) compounds as a function of temperature is shown in Fig. 9 at different pressures.

We see that the α coefficient of the three compounds increases rapidly in the interval between 0 and 400 K. Beyond this value of 400 K, we see that it undergoes a slight increase towards to a limited value. The α coefficient of the Mg_3FeO_4, Ca_3FeO_4 and Se_3FeO_4 compounds at ambient temperature and pressure ($T = 300$ K and $p = 0$ GPa) are respectively equal to 3.25×10^{-5}, 4.72×10^{-5} and 5.71×10^{-5} K^{-1}.

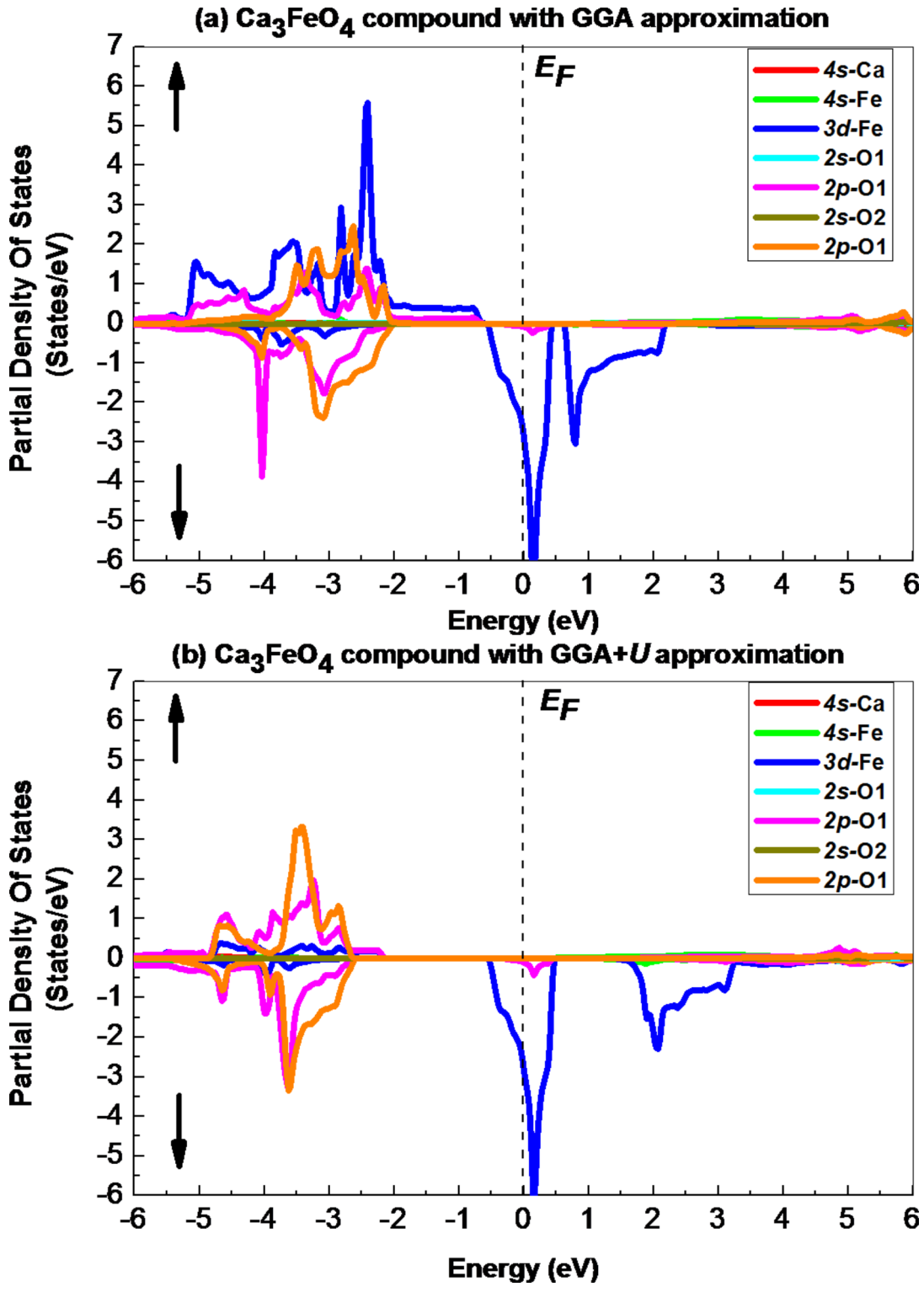

Fig. 7. Calculation of the spin-dependent partial density of states (PDOS) of the material Ca_3FeO_4, applying the (**a**) PBE-GGA and (**b**) GGA + *U* schemes.

The heat capacity at constant volume C_V of the three studied compounds has a behavior proportional to T^3 in the temperature range from 0 to 300 K; it reaches the Dulong and Petit limit in the high temperature range. The C_V values of the equilibrium Mg_3FeO_4, Ca_3FeO_4 and Se_3FeO_4 at ambient temperature and pressure are found to be: 154.17 J mol^{-1} K^{-1}, 170.31 J mol^{-1} K^{-1} and 183.33 J mol^{-1} K^{-1}, respectively.

The Debye temperature θ_D is an important factor that must be determined, because above this temperature the solid will have a classical behavior due to the thermal vibrations which manifest much more than the

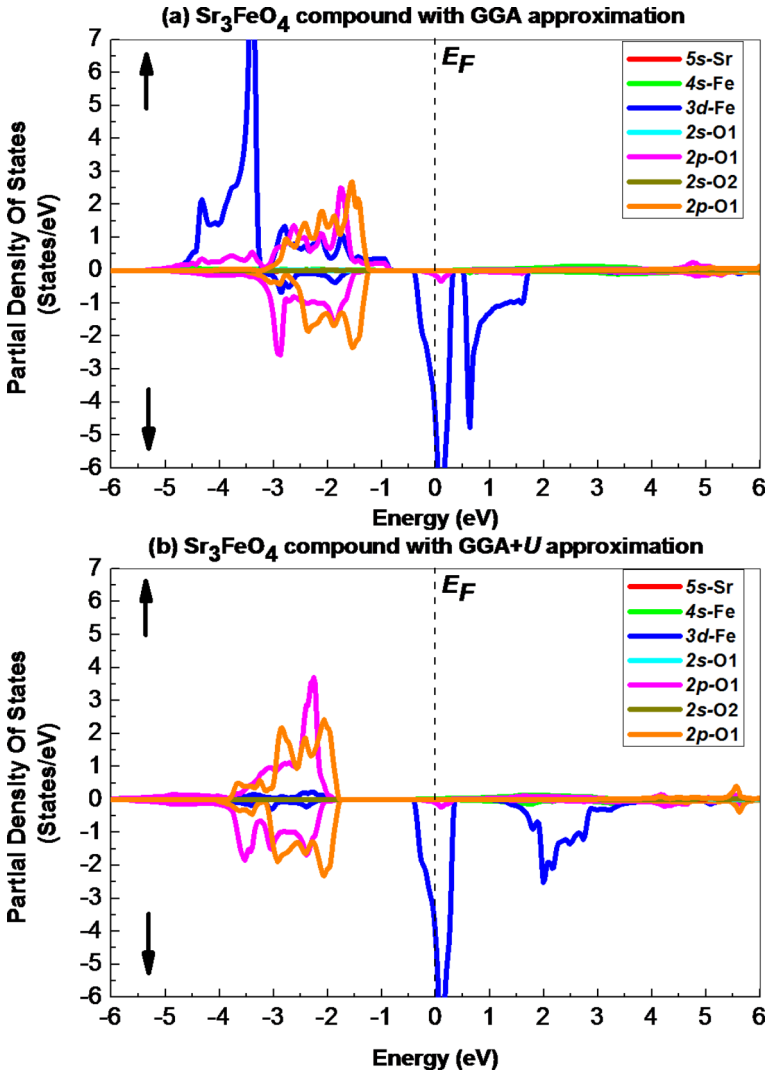

Fig. 8. Calculation of the spin-dependent partial density of states (PDOS) of the material Sr_3FeO_4, applying the (**a**) PBE-GGA and (**b**) GGA + *U* schemes.

Compound	Magnetic moment (μ_B)						Curie temperature	
	M_{Tot}	Interstitial	X	Fe	O1	O2	$\Delta E = E_{AFM} - E_{AFM}$ (eV)	T_C (K)
Mg_3FeO_4	3.9949 (4.0019)	0.1314 (0.0562)	-0.0011 (-0.0015)	3.5000 (3.7019)	0.1216 (0.0829)	0.0018 (-0.0000)	0.2176	832.4592
Ca_3FeO_4	4.0056 (4.0007)	0.0905 (0.0085)	-0.0039 (-0.0048)	3.5634 (3.7711)	0.1217 (0.0787)	-0.0006 (-0.0008)	0.2635	989.8945
Sr_3FeO_4	4.0043 (4.0008)	0.0464 (0.0045)	-0.0037 (-0.0044)	3.5965 (3.8278)	0.1224 (0.0601)	0.0053 (0.0014)	0.4016	1490.1072

Table 5. Calculations of the total magnetic moment M_{Tot} (in μ_B), the magnetic moment in the interstitial zone, the Curie temperature T_C (in K) and the local magnetic moment of each site of the X_3FeO_4 (X = mg, ca and Sr) compounds, the values of GGA + *U* are in parentheses.

quantum effects. The θ_D factor of all the studied compounds decreases slowly in the temperature range from 0 to 200 K; it then undergoes a drastic linear decrease as a function of temperature (see Fig. 8 (c)). The θ_D values of all the equilibrium X_3FeO_4 (X = Mg, Ca and Sr) compounds at ambient temperature and pressure are determined to be: 704.15 K, 572.51 K and 422.02 K, respectively.

Sound velocities

In the cubic crystal, the elastic sound velocities which propagate along the [100], [110] and [111] directions are determined only by the three independent elastic constants C_{11}, C_{12} and C_{44}[58].

In the case of the elastic waves that propagate along the [100] direction, the longitudinal (u_1 in direction of propagation and $u_2 = u_3 = 0$) and transverse ($u_1 = 0$ and u_2 and u_3 perpendicular to the direction of propagation) elastic waves have respectively the velocities which are expressed as follows[58,59]:

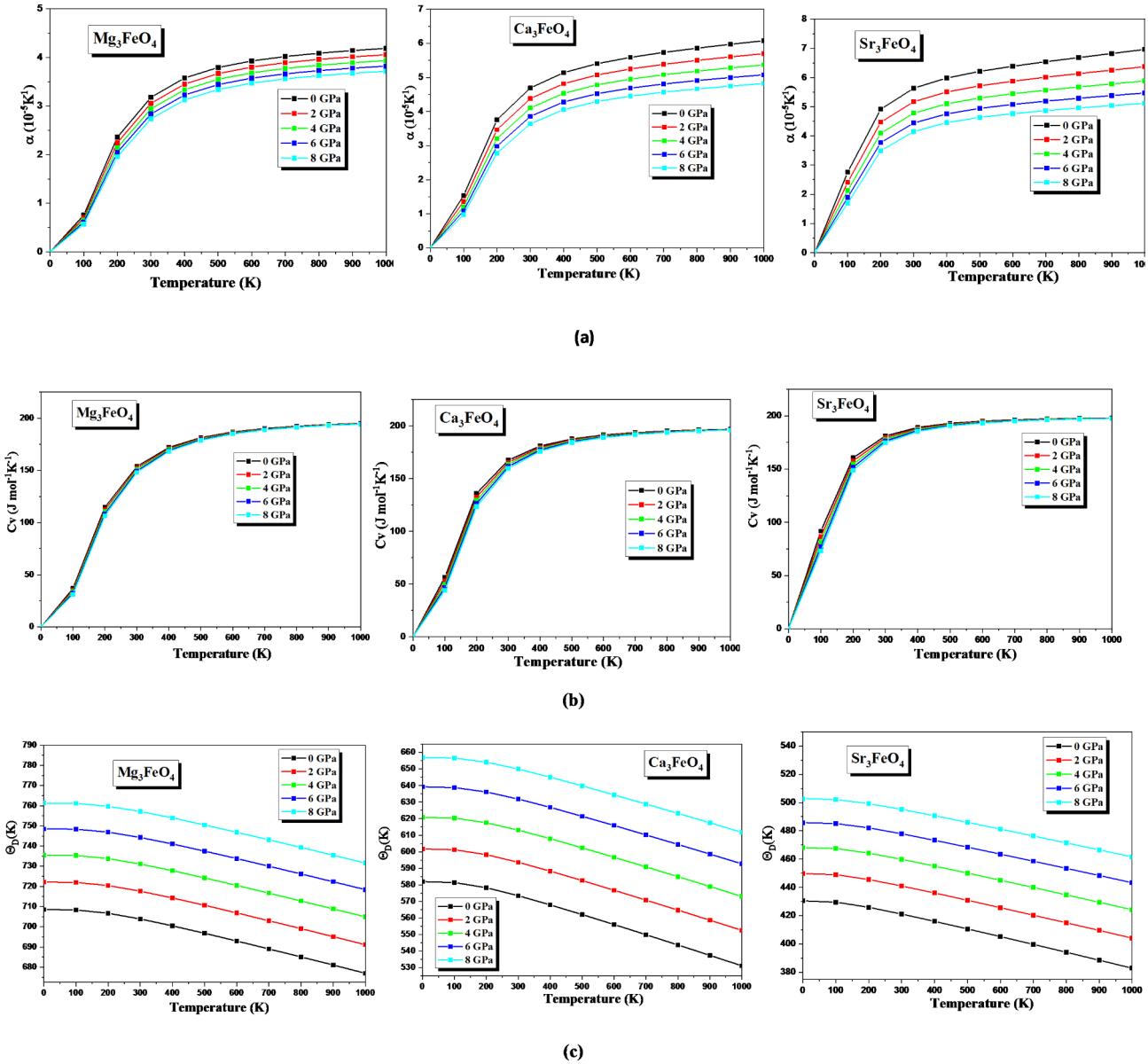

Fig. 9. Variation of: (**a**) the thermal expansion coefficient (α), (**b**) the heat capacity at constant volume (C_V) and (**c**) the Debye temperature (θ_D) of the X_3FeO_4 (X = Mg, Ca and Sr) compounds versus temperature and at different pressures, using the GGA approximation.

$$\begin{cases} v_l = \sqrt{C_{11}/\rho} \\ v_{t1} = v_{t2} = \sqrt{C_{44}/\rho} \end{cases} \tag{12}$$

In the case of the elastic waves that propagate in the [110] direction, the velocities are given in the following formulas[46,47]:

$$\begin{cases} v_l = \sqrt{(C_{11} + C_{12} + 2C_{44})/2\rho} \\ v_{t1} = \sqrt{(C_{11} - C_{12})/2\rho} \\ v_{t2} = \sqrt{C_{44}/\rho} \end{cases} \tag{13}$$

In the case of the elastic waves that propagate along the [111] direction, the velocities of the longitudinal ($u_1 = u_2$ and $u_3 = 0$) and transverse ($u_1 = u_2 = u_3$) elastic waves are expressed in the following relations:

$$\begin{cases} v_l = \sqrt{(C_{11} + 2C_{12} + 4C_{44})/3\rho} \\ v_{t1} = v_{t2} = \sqrt{(C_{11} - C_{12} + C_{44})/3\rho} \end{cases} \tag{14}$$

Compound	Crystal density ρ (g/cm³)	Direction	Polarization	Sound velocity type	Sound velocity value (m/s)
Mg_3FeO_4	4.0550	[100] [110] [111]	[100] [010] ≡ [001] [11$\bar{0}$] [1 1 0] [001] [11$\bar{1}$] [11 2]	v_l $v_{t1} = v_{t2}$ v_l v_{t1} v_{t2} v_l $v_{t1} = v_{t2}$	7923.9947 5379.6484 8542.5785 4330.6652 5379.6484 8739.0483 4706.3765
Ca_3FeO_4	3.7250	[100] [110] [111]	[100] [010] ≡ [001] [11$\bar{0}$] [1 1 0] [001] [11$\bar{1}$] [11 2]	v_l $v_{t1} = v_{t2}$ v_l v_{t1} v_{t2} v_l $v_{t1} = v_{t2}$	8106.8535 5212.6202 8231.9381 5012.7515 5212.6202 8273.2127 5080.2482
Sr_3FeO_4	4.9684	[100] [110] [111]	[100] [010] ≡ [001] [11$\bar{0}$] [1 1 0] [001] [11$\bar{1}$] [11 2]	v_l $v_{t1} = v_{t2}$ v_l v_{t1} v_{t2} v_l $v_{t1} = v_{t2}$	6047.5421 4223.6847 6429.6703 3615.4693 4223.6847 6552.0957 3828.9576

Table 6. GGA calculations of the sound velocities (in m/s) for the equilibrium X_3FeO_4 (X = mg, ca and Sr) compounds along the [100], [110] and [111] directions, where v_l and v_t are respectively the velocities of longitudinal acoustic waves and transverse acoustic waves.

Where, ρ is the crystal density.

The sound velocities calculated by the GGA approximation for the equilibrium X_3FeO_4 (X = Mg, Ca and Sr) compounds along the [100], [110] and [111] directions are grouped in Table 6. For comparison, there are no experimental or theoretical data available in the literature for these compounds, so our sound velocity values are considered as a pioneering reference for further researches.

Conclusions

In this study, the FP-LAPW + lo method was adopted in order to predict the different physical properties of the X_3FeO_4 (X = Mg, Ca and Sr) compounds, where the GGA and GGA + *U* schemes defined the exchange and correlation potential of this *ab* initio method. The main conclusions of this approach are given as follows:

- The study of structural properties developed by the GGA approximation shows that the stable ground state of all the studied compounds is reported in the ferromagnetic phase, where their equilibrium lattice parameters are optimized for each magnetic phase.
- The elastic constants were calculated using the GGA approximation for each material taken in its stable phase in order to confirm their mechanical stability with respect to the Born criteria; the anisotropy factor shows that the compounds are elastically anisotropic ($A \neq 1$).
- The Pugh's ratio and Poisson ratio calculated for all the studied compounds prove that they are brittle materials ($B_0/G < 1.75$ and $\upsilon < 0.33$).
- The GGA + *U* results of the electronic properties of all the studied compounds show that these materials have a perfect half-metallic electronic structure with a large half-metallic gap (more than 0.28 eV).
- Finally, GGA and GGA + *U* calculations of the magnetic properties of the different compounds show that:

i. The total magnetic moment of each material is integer (of 4 μ_B), confirming the half-metallic character of these studied compounds.
ii. The magnetic moments of Fe and X atoms are found in opposite signs; this means that the valence electrons of Fe and X atoms interact anti-ferromagnetically during the exchange and splitting process.
iii. The hybridization between the *3d*-Fe and *2p*-O orbitals is responsible for reducing the magnetic moment of the Fe atom relative to its free magnetic moment and producing of small magnetic moments to the non-magnetic sites of the X and O atoms.
iv. Furthermore, these materials are marked by a high Curie temperature (more than 832 K).

Data availability

The datasets used and/or analyzed during the current study available from the corresponding author (fatmimessaoud@yahoo.fr) on reasonable request.

Received: 16 November 2024; Accepted: 20 January 2025
Published online: 23 January 2025

References

1. Pickett, W. E. & Moodera, J. S. *Phys. Today* **54**, 39–44 (2001).
2. de Groot, R. A., Mueller, F. M., van Engen, P. G. & Buschow, K. H. J. *Phys. Rev. Lett.* **50**, 2024–2027 (1983).
3. Kobayashi, K. L., Kimura, T., Sawada, H., Terakuraand, K. & Tokura, Y. *Nature* **395**, 677–680 (1998).
4. Soulen, R. J. Jr et al. J.M.D, Science 282 85–88. (1998).

5. Wurmehl, S. et al. *Appl. Phys. Lett.* **88**, 032503 (2006).
6. Galanakis, I. *Phys. Rev. B* **71**, 012413 (2005).
7. Ohno, H. et al. *Phys. E* **2**, 904–908 (1998).
8. Haoui, A., Elchikh, M., Hiadsi, S., Hireche, A. & Baghdad *Phys. B* **684**, 416001 (2024).
9. Ati, A. H. et al. Khalaf Al-zyadi. *J. Phys. Chem. Solids*. **188**, 111899 (2024).
10. Wei, W., Lee, P-H. & Wang, Y-K. *Chin. J. Phys.* **89**, 1763–1770 (2024).
11. Wei, X-P., Mei, Z-Y. & Tao, X. *Phys. B*, **683**, 41595 (2024).
12. Belhadj, M. E. A. et al. *Comput. Theor. Chem.*, **1234**, 114526 (2024).
13. Zhang, Z. et al. *J. Alloys Compd.*, **967**, 171643 (2023).
14. Zhai, M-X., Liang, X. & Li, D-X. *Results Phys.*, **39**, 105733 (2022).
15. Mehra, P., Saini, H. S., Sinhmar, S., Thakur, J. & Kashyap, M. K. *Vacuum* **182**, 109760 (2020).
16. Jafarova, V. N. *Solid State Commun.*, **369**, 115197 (2023).
17. Rahmathulla, S. S. & Sirajuddeen, M. M. S. *Mater. Chem. Phys.*, **243**, 122336 (2020).
18. Yan, Z., Wu, H. & Zheng, R. *Comput. Mater. Sci.*, **99**, 16–20 (2015).
19. Garg, S., Gautam, S., Singh, J. P., Kandasami, A. & Goyal, N. *Mater. Charact.* **179**, 111366 (2021).
20. Parrey, K. A., Farooq, T., Khandy, S. A., Farooq, U. & Gupta, A. *Comput. Condens. Matter*, **19**, e00381 (2019).
21. Jamil, M. et al. *Solid State Commun.*, **394**, 115702 (2024).
22. Sofi, M. Y., Khan, M. S. & Khan, M. A. *Mater. Sci. Semiconduct. Process.*, **186**, 10902. (2025).
23. Tanveer, W. et al. *Mater. Sci. Eng., B*, **310**, 117772 (2024).
24. Liu, Z. et al. Fundamental Research, https://doi.org/10.1016/j.fmre.2024.11.024
25. Yasir, M. A. et al. *Mater. Sci. Eng., B*, **311**, 117830 (2025).
26. Vensky, S. et al. *Z. Kristallogr.* **220**, 231–244 (2005).
27. Wong, K. M., Alay-e-Abbas, S. M., Shaukat, A., Fang, Y. & Lei, Y. *J. Appl. Phys.* **113**, 014304 (2013).
28. Wong, K. M., Alay-e-Abbas, S. M., Fang, Y., Shaukat, A. & Lei, Y. *J. Appl. Phys.* **114**, 034901 (2013).
29. Blaha, P., Schwarz, K., Sorantin, P. & Trickey, S. K. *Comput. Phys. Commun.* **59**, 339 (1990).
30. Hohenberg, P. & Kohn, W. *Phys. Rev.* **136**, B864 (1964).
31. Perdew, J. P., Burke, S. & Ernzerhof, M. *Phys. Rev. Lett.* **77**, 3865–3868 (1996).
32. Anisimov, V. I., Solovyev, I. V., Korotin, M. A., Czyzyk, M. T. & Sawatzky, G. A. *Phys. Rev. B* **48**, 16929 (1993).
33. Togo, A. & Tanaka, I. *Scr. Mater.* **108**, 1 (2015).
34. Murnaghan, F. D. Proc. Natl. Acad. Sci. 30 244–247. (1944).
35. Shang, S. L., Wang, Y., Kim, D. & Liu, Z. K. *Comput. Mater. Sci.* **47**, 1040–1048 (2010).
36. Yakoubi, A., Baraka, O. & Bouhafs, B. *Results Phys.* **2**, 58–65 (2012).
37. Zeng, Z. H., Calle-Vallejo, F., Mogensen, M. B. & Rossmeisl, J. *Phys. Chem. Chem. Phys.* **15**, 7526–7533 (2013).
38. Rai, D. P. et al. *RSC Adv.* **5**, 95353–95359 (2015).
39. Smallwood, J. C. *Phys. Rev.* **33**, 317 (1911).
40. Kramers–kronig, J. B. *Am. J. Phys.* **79**, 1053–1059 (2011).
41. Born, M. & Huang, K. *Dynamical Theory of Crystal Lattices* (Clarendon, 1956).
42. Wang, J. & Yip, S. *Phys. Rev. Lett.* **71**, 4182 (1993).
43. Chen, H., Yang, L. & Long, J. *Superlattices Microstruct.*, **79**, 156–165 (2015).
44. Voigt, W. *Lehrbuch Der Kristallphysik* (Taubner, 1928).
45. Reuss, A. & Angew, Z. *Math. Mech.* **9**, 55 (1929).
46. Hill, R. Proc. Phys. Soc. Lond. 65 909. (1953).
47. Vaitheeswaran, G. et al. *Phys. Rev. B* **76**, 014107 (2007).
48. Pugh, S. F. *Philos. Mag* **45**, 823 (1954).
49. Simmon, G. & Wang, H. *Single Crystal Elastic Constants and Calculated Aggregate Properties: A Handbook* (M.IT, 1971).
50. Fu, H., Li, D., Peng, F., Gao, T. & Cheng, X. *Comput. Mater. Sci.* **44**, 774 (2008).
51. Kleinman, L. *Phys. Rev.*, **128**(6), 2614–2621 (1962).
52. Yao, K. L., Gao, G. Y., Liu, Z. L. & Zhu, L. *Solid State Commun.* **133**, 301–304 (2005).
53. Gao, G. Y. et al. *Phys. Rev. B* **75**, 174442 (2007).
54. Zunger, A. *Solid State Phys. : Condens. Matter* **39**, 275 (1986).
55. Cui, X. Y., Delley, B., Freeman, A. J. & Stampfl, C. *Phys. Rev. Lett.* **97**, 016402 (2006).
56. Kubler, J., Fecher, G. H. & Felser, C. *Phys. Rev. B* **76**, 024414 (2007).
57. Blanco, M. A., Francisco, E. & Luaña, V. *Comput. Phys. Commun.* **158**, 57–72 (2004).
58. Adachi, S., Properties of Group-IV, III-V and & Semiconductors, I. I. V. I. John Wiley & Sons, England, ISBN 0-470-09032-4. (2005).
59. Lüthi, B. Physical Acoustics in the Solid State, Springer-Verlag Berlin Heidelberg, ISBN 978-3-540-72193-2. (2007).

Acknowledgements

The authors extend their appreciation to the Deanship of Scientific Research at Northern Border University, Arar, KSA for funding this research work through the project number NBU-FFR-2025-310-04.

Author contributions

Conceptualization: Mohammed El Amine MonirData curation: Abdelkarim Bendoukha ReguigFormal analysis; Validation: Faisal Katib Alanazi, M. FatmiMethodology: M.A. GhebouliSoftware: K. Bouferrache, H. Bouandas.

Declarations

Competing interests

The authors declare no competing interests.

Additional information

Correspondence and requests for materials should be addressed to F.K.A. or M.F.

Reprints and permissions information is available at www.nature.com/reprints.

Publisher's note Springer Nature remains neutral with regard to jurisdictional claims in published maps and institutional affiliations.